

# Reason-IAD: Knowledge-Guided Dynamic Latent Reasoning for Explainable Industrial Anomaly Detection

Peng Chen<sup>1</sup> Chao Huang<sup>\*1</sup> Yunkang Cao<sup>2</sup> Chengliang Liu<sup>3</sup> Wenqiang Wang<sup>1</sup> Mingbo Yang<sup>1</sup> Li Shen<sup>1</sup>  
Wenqi Ren<sup>1</sup> Xiaochun Cao<sup>1</sup>

## Abstract

Industrial anomaly detection demands precise reasoning over fine-grained defect patterns. However, existing multimodal large language models (MLLMs), pretrained on general-domain data, often struggle to capture category-specific anomalies, thereby limiting both detection accuracy and interpretability. To address these limitations, we propose Reason-IAD, a knowledge-guided dynamic latent reasoning framework for explainable industrial anomaly detection. Reason-IAD comprises two core components. First, a retrieval-augmented knowledge module incorporates category-specific textual descriptions into the model input, enabling context-aware reasoning over domain-specific defects. Second, an entropy-driven latent reasoning mechanism conducts iterative exploration within a compact latent space using optimizable latent think tokens, guided by an entropy-based reward that encourages confident and stable predictions. Furthermore, a dynamic visual injection strategy selectively incorporates the most informative image patches into the latent sequence, directing the reasoning process toward regions critical for anomaly detection. Extensive experimental results demonstrate that Reason-IAD consistently outperforms state-of-the-art methods. The code will be publicly available at <https://github.com/chenpeng052/Reason-IAD>.

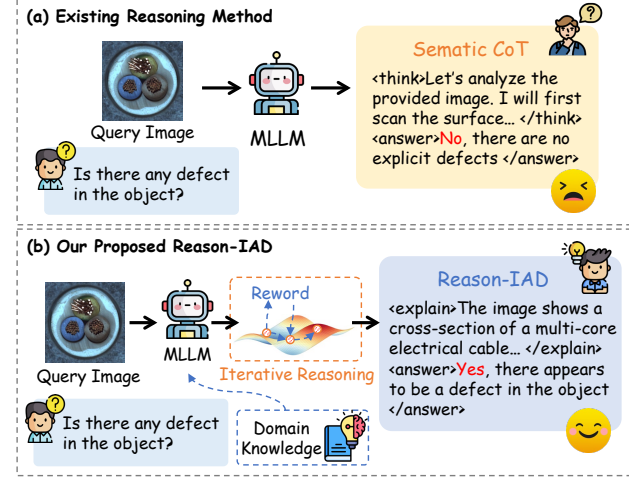


Figure 1. Comparison between existing reasoning methods and the proposed Reason-IAD. (a) Existing methods conduct reasoning through explicit chains of thought. (b) Reason-IAD retrieves domain-specific knowledge and identifies anomalies via iterative latent reasoning.

## 1. Introduction

Industrial anomaly detection plays a critical role in ensuring the safety and reliability of modern manufacturing systems (Jiang et al., 2024; Zhang et al., 2025a; Fang et al., 2024), aiming to accurately identify anomalous samples that deviate from normal patterns in complex visual data (Ma et al., 2025; Wang et al., 2025b). However, conventional methods typically rely on carefully curated, task-specific datasets, rendering them highly sensitive to domain priors and limiting their generalization across diverse scenarios and product categories (Cao et al., 2024; Qu et al., 2025). In practice, substantial distribution discrepancies across different industrial products and imaging conditions introduce severe domain shifts, hindering their deployment in real-world manufacturing environments.

In recent years, vision-language models have demonstrated considerable potential for industrial anomaly detection due to their strong multimodal representation and generalization capabilities (Qu et al., 2024; Ma et al., 2025). CLIP-based

<sup>1</sup>School of Cyber Science and Technology, Shenzhen Campus of Sun Yat-sen University, Shenzhen, China <sup>2</sup>School of Artificial Intelligence and Robotics, Hunan University, Changsha, China <sup>3</sup>Department of Computer and Information Science, University of Macau, Macau, China. Correspondence to: Chao Huang <huangch253@mail.sysu.edu.cn>.

approaches align visual features with textual semantics, enabling anomaly detection under zero-shot and few-shot settings (Yan et al., 2025). For instance, AnomalyCLIP (Zhou et al., 2023) introduces category-agnostic textual embeddings to reduce reliance on manually designed priors, while AdaCLIP (Cao et al., 2024) and BayPFL (Qu et al., 2025) replace static prompts with learnable textual embeddings to enhance semantic expressiveness and model adaptability. Despite these advances, the performance of such methods remains constrained by the representational capacity of pre-trained models (Jeong et al., 2023; Li et al., 2024b; Wang et al., 2025b). When confronted with complex industrial scenes and fine-grained defect patterns, they often fail to achieve reliable anomaly recognition (Gu et al., 2024a; Qu et al., 2024). Moreover, these approaches generally lack explicit reasoning mechanisms, preventing evidence-based analysis as human experts would do, thus limiting their applicability in high-reliability industrial scenarios.

Recent advances in multimodal large language models (MLLMs) have opened a promising avenue for developing general-purpose, expert-level industrial anomaly detection systems (Gu et al., 2024b; Li et al., 2025c), owing to their strong pretraining and reasoning capabilities (Yan et al., 2025; Tan et al., 2025a). MMAD (Jiang et al., 2024) introduced the first systematic benchmark for anomaly detection reasoning, evaluating models' reasoning abilities across multiple dimensions. Building on this, Anomaly-R1 (Chao et al., 2025) leverages the GRPO training strategy to construct an end-to-end anomaly detection framework that replaces traditional expert systems, while AD-FM (Liao et al., 2025) adopts a two-stage reasoning paradigm, combining supervised fine-tuning (SFT) with GRPO to progressively adapt pre-trained multimodal models to anomaly detection tasks. However, as illustrated in Figure 1 (a), these approaches typically rely on explicitly generating long reasoning chains (chain-of-thought) to reach decisions, resulting in substantial inefficiency and limited scalability (Sun et al., 2025; Li et al., 2025a). Furthermore, since the underlying models are primarily pre-trained on general-domain data, they often lack task-specific domain knowledge for industrial anomaly detection, which constrains the reliability and stability of their reasoning outcomes.

To address these challenges, we propose Reason-IAD, a training-free framework for explainable industrial anomaly detection that leverages knowledge-guided dynamic latent reasoning. As illustrated in Figure 1(b), Reason-IAD consists of two key components. First, a retrieval-augmented knowledge module incorporates category-specific textual descriptions into the model input, enabling context-aware reasoning over domain-specific defects. Second, an entropy-driven latent reasoning mechanism conducts iterative exploration within a compact latent space using optimizable latent think tokens, facilitating confident and stable reasoning.

In addition, a dynamic visual injection strategy selectively injects the most informative image regions into the latent sequence, guiding the reasoning process toward critical visual evidence for anomaly detection. We evaluate Reason-IAD across seven sub-tasks under one-shot and zero-shot settings. Extensive experiments demonstrate that Reason-IAD consistently outperforms existing methods, highlighting its effectiveness and interpretability.

Our main contributions are summarized as follows:

- To the best of our knowledge, this is the first work to leverage MLLMs for training-free reasoning in the context of industrial anomaly detection.
- We propose Reason-IAD, a knowledge-guided dynamic latent reasoning framework for explainable industrial anomaly detection, enabling effective anomaly perception through iterative reasoning guided by visual evidence and entropy-driven reward optimization.
- Extensive experiments demonstrate the effectiveness and generality of Reason-IAD, providing an efficient and practical solution for applying MLLMs to industrial anomaly detection.

## 2. Related Work

### 2.1. Anomaly Detection

Anomaly detection aims to identify abnormal patterns that deviate from the normal data distribution (Ma et al., 2025; Liao et al., 2025; Chen et al., 2026). However, substantial variability in appearance and the scarcity of anomalous samples make anomaly detection a particularly challenging task (Gu et al., 2024a; Yan et al., 2025; Feng et al., 2025). To address these challenges, traditional unsupervised methods learn representations solely from normal samples and identify anomalies during testing (Roth et al., 2022; Deng & Li, 2022; Zhang et al., 2025b). While effective to some extent, these approaches often rely on category-specific models, which constrain their generalization and practical applicability in real-world industrial scenarios.

Recent studies have explored vision-language models for zero-shot and few-shot anomaly detection by aligning visual representations with textual semantics (Qu et al., 2024; Xu et al., 2025; Qu et al., 2025). For example, WinCLIP (Jeong et al., 2023) leverages CLIP (Radford et al., 2021) to compute similarities between multi-scale image patch features and manually designed textual prompts for anomaly discrimination. To enable more flexible and adaptive cross-modal alignment, methods such as AdaCLIP (Cao et al., 2024) and BayPFL (Qu et al., 2025) further incorporate image information into the prompt construction process, enhancing the model's capacity to capture anomaly-related semantics.

Despite the performance gains of these approaches, their inference pipelines predominantly rely on static similarity matching, and the limited reasoning capability of the base models remains a critical bottleneck.

## 2.2. Visual Reasoning

Visual reasoning is a fundamental challenge in artificial general intelligence, requiring models to perform complex cognitive reasoning grounded in visual perception (Wang et al., 2025a; Ding & Zhang, 2025). This capability is essential for a wide range of tasks, including visual counting, geometric problem solving, and anomaly detection (Shi et al., 2025; Chen et al., 2025a; Wan et al., 2025). Early approaches primarily relied on program synthesis or neuro-symbolic reasoning frameworks (Amizadeh et al., 2020; Gupta & Kembhavi, 2023). In contrast, recent advances in vision-language models have enabled the integration of large language models to enhance visual reasoning, attracting increasing research interest. Representative works such as Reason-RFT (Tan et al., 2025a) adopt a two-stage training strategy combining supervised fine-tuning and reinforcement learning to improve visual reasoning. In anomaly detection, Anomaly-R1 (Chao et al., 2025) integrates multimodal large language models with a GRPO-based reasoning alignment mechanism to enhance output consistency and reliability. AD-FM (Liao et al., 2025) introduces a two-stage paradigm bridging anomaly perception and explanation, enabling more interpretable reasoning. Additionally, Triad (Li et al., 2025d) incorporates expert-guided anomalous region awareness with chain-of-thought reasoning, significantly improving defect perception and reasoning performance in industrial anomaly detection. However, most existing approaches rely heavily on large-scale reconstructed datasets for fine-tuning, resulting in high training costs and limited scalability in real-world industrial settings.

## 2.3. Latent Reasoning

Recent research on advanced reasoning in multimodal large language models (MLLMs) has evolved from explicit text-based reasoning toward more efficient latent space reasoning approaches (Sun et al., 2025; Tan et al., 2025b; Li et al., 2025b). In latent space reasoning, the intermediate “thinking process” is encoded as continuous vectors in the model’s hidden space rather than as discrete textual representations, aiming to achieve performance comparable to explicit chain-of-thought (CoT) reasoning while using a more compact and efficient representation (Chen et al., 2025b; Ruan et al., 2025; Geiping et al., 2025). Some methods enhance latent representations through carefully designed training strategies to enable more effective interactive reasoning (Hao et al., 2024; Yang et al., 2025; Huang et al., 2025), while others adopt training-free approaches that guide latent activations to refine the reasoning process (Zhang et al., 2025c;

Liu et al., 2025; Pham & Ngo, 2025). Despite these advances, existing methods generally lack knowledge-guided reasoning and the integration of visual context, limiting their effectiveness on tasks that require external knowledge or visual evidence. In contrast, our approach retrieves relevant knowledge and dynamically integrates visual evidence into the latent reasoning process, substantially enhancing performance in industrial anomaly detection.

## 3. Methodology

### 3.1. Problem Definition

In this work, we study a multimodal anomaly detection question-answering (QA) task, in which the model answers questions based on a given industrial image.

Formally, given a query image  $I \in \mathcal{I}_{test}$  depicting an industrial object and a question  $Q \in \mathcal{Q}_{test}$ , the model aims to predict the correct answer  $A$ . Each question corresponds to a specific anomaly reasoning objective, demanding varying levels of visual perception and reasoning.

Our proposed method supports anomaly detection under two settings:

- **One-shot setting:** the model receives a query image  $I$  and a question  $Q$ , along with a reference image  $I_r \in \mathcal{I}_{ref}$  of a normal object from the same domain. The model is required to generate both the answer and a corresponding explanation.
- **Zero-shot setting:** the model only receives the query image  $I$  and the question  $Q$ , without any reference information, and is expected to produce the answer along with the relevant explanation.

### 3.2. Reason-IAD

In this paper, we propose Reason-IAD, a knowledge-guided dynamic latent reasoning framework for explainable industrial anomaly detection. As illustrated in Figure 2, Reason-IAD comprises two principal components: (1) a Retrieval-Augmented Knowledge Integration (RAKI) module that retrieves category-specific textual descriptions and incorporates them into the model prompt, enabling context-aware reasoning over domain-specific defects; and (2) an Entropy-Driven Latent Reasoning mechanism (EDLR) that performs iterative exploration in a compact latent space using optimizable latent think tokens. Furthermore, inspired by human cognitive behavior in revisiting visual evidence under uncertainty, we introduce a dynamic visual injection strategy that selectively incorporates the most informative image patches into the latent sequence, guiding the reasoning process toward regions that are critical for anomaly detection.

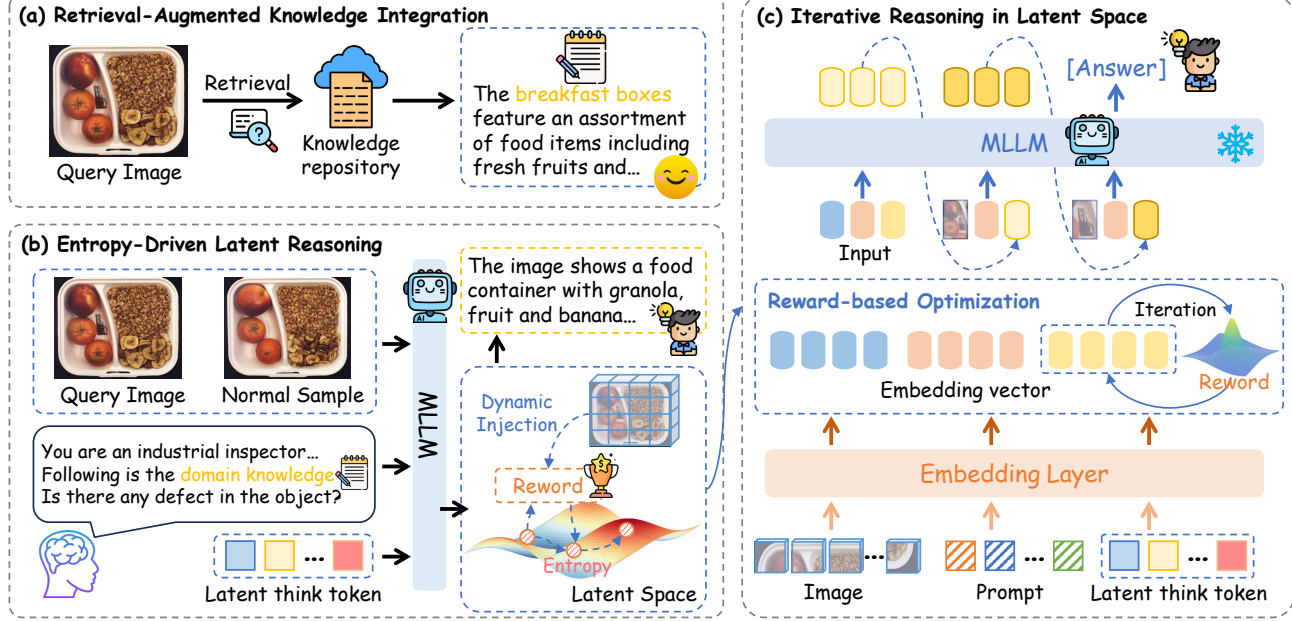


Figure 2. Overview of the proposed Reason-IAD. (a) Given a query image, Reason-IAD retrieves the most relevant category-specific descriptions and incorporates them into the model prompt to enhance anomaly awareness. (b) An entropy-guided latent reasoning module iteratively refines latent think tokens and dynamically injects visual evidence to improve reasoning accuracy. (c) Illustration of the iterative latent-space reasoning process, in which reward signals and visual cues progressively guide the model toward the final prediction.

### 3.3. Retrieval-Augmented Knowledge Integration

Existing multimodal large language models are predominantly pretrained on general-domain data, which often limits their ability to understand industrial anomalies. To improve both reasoning accuracy and explainability in industrial anomaly detection tasks, we propose a retrieval-augmented mechanism that incorporates category-specific knowledge to enrich the model input prompt.

Specifically, given a query image  $I$  and its associated question  $Q$ , we construct a category-oriented knowledge repository  $\mathcal{K} = \{(c_i, \text{desc}_i)\}_{i=1}^N$ , where  $c_i$  denotes the  $i$ -th category label (e.g., cable, breakfast box), and  $\text{desc}_i$  provides a detailed textual description of the category, encompassing both normal characteristics and defect patterns. This repository serves as an external knowledge source for contextual augmentation. To identify the most relevant category information, the query image is first encoded into a visual embedding  $\mathbf{v} \in \mathbb{R}^d$  using a visual encoder  $f_v$ , while each category label  $c_i$  is encoded into a textual embedding  $\mathbf{k}_i \in \mathbb{R}^d$  using a text encoder  $f_t$ , projecting both modalities into a shared semantic space:

$$\mathbf{v} = f_v(I), \quad \mathbf{k}_i = f_t(c_i). \quad (1)$$

We then evaluate the semantic alignment between the query image and each category label by computing their cosine

similarity:

$$s_i = \frac{\mathbf{v}^\top \mathbf{k}_i}{\|\mathbf{v}\| \|\mathbf{k}_i\|}, \quad i = 1, \dots, N, \quad (2)$$

where  $s_i$  denotes the similarity score between the query image and the  $i$ -th category. According to the similarity scores  $\{s_i\}$ , we retrieve the top- $k$  categories with the highest scores. The corresponding category descriptions are then incorporated into the model input prompt, forming an enriched contextual representation that provides category-aware guidance for reasoning and explanation generation.

### 3.4. Entropy-Driven Latent Reasoning

Industrial anomaly detection often demands sophisticated reasoning over subtle visual patterns and contextual knowledge. Traditional approaches, such as Chain-of-Thought (CoT) prompting, rely on generating explicit textual reasoning steps to guide model predictions, but they typically entail lengthy intermediate reasoning processes. Inspired by the intertwined nature of perception and reasoning in human cognition, we propose Reason-IAD, an entropy-driven latent reasoning framework. Within this framework, the model dynamically integrates visual evidence from the query image with category-specific knowledge from an external repository in the latent space, producing a compact and interpretable reasoning representation that enables robust industrial anomaly detection.

**Algorithm 1** Reason-IAD: Knowledge-Guided Dynamic Latent Reasoning

---

```

1: Input: Query image  $I$ , question  $Q$ , knowledge repository  $\mathcal{K} = \{(c_i, \text{desc}_i)\}_{i=1}^N$ , latent token number  $m$ , iteration number  $N_{\text{iter}}$ , top- $k$  categories
2: Encode image:  $\mathbf{v} \leftarrow f_v(I)$ 
3: for each category  $c_i \in \mathcal{K}$  do
4:   Encode text:  $\mathbf{k}_i \leftarrow f_t(c_i)$ 
5:   Compute similarity:  $s_i \leftarrow \cos(\mathbf{v}, \mathbf{k}_i)$ 
6: end for
7: Retrieve top- $k$  categories  $\{c_{(1)}, \dots, c_{(k)}\}$  by  $\{s_i\}$  and Construct enriched prompt
8: Initialize latent think tokens  $\mathcal{Z} = \{z_1, \dots, z_m\}$ 
9: for  $n = 1$  to  $N_{\text{iter}}$  do
10:   Sample noise  $\xi^{(n)} \sim \mathcal{N}(0, \sigma^2 I)$ 
11:    $\mathcal{Z}'^{(n)} \leftarrow \mathcal{Z}^{(n)} + \eta \nabla_{\mathcal{Z}^{(n)}} J(\mathcal{Z}^{(n)})$ 
12:   Initialize best patch  $V_{\text{best}}$ 
13:   for  $j = 1, \dots, m$  do
14:     Sample candidate patches  $V_{\text{cand}}$  according to attention distribution
15:     Compute entropy  $\mathcal{H}^{(n)}$  and reward  $\mathcal{R}^{(n)}$  using Eq. (5)–(6)
16:     if  $\mathcal{R}^{(n)} > \mathcal{R}_{\text{best}}$  then
17:        $V_{\text{best}} \leftarrow V_{\text{cand}}$ 
18:        $\mathcal{R}_{\text{best}} \leftarrow \mathcal{R}^{(n)}$ 
19:     end if
20:   end for
21: end for
22: Return reasoning result

```

---

**Latent Think Tokens.** To facilitate dynamic exploration in the latent space, we introduce a set of latent think tokens, denoted as  $\mathcal{Z} = \{z_1, z_2, \dots, z_m\}$ , which are initialized as optimizable vector embeddings and inserted into the original multimodal input sequence. During each iteration of latent reasoning, we incorporate controlled stochasticity to expand the search space while preserving the stability of the representations. Specifically, we adopt additive Gaussian noise as a local perturbation strategy. Given the latent think tokens  $\mathcal{Z}^{(n)}$  at iteration  $n$ , the perturbed state is defined as:

$$\mathcal{Z}'^{(n)} = \mathcal{Z}^{(n)} + \xi^{(n)}, \quad \xi^{(n)} \sim \mathcal{N}(0, \sigma^2 I), \quad (3)$$

where  $\sigma^2$  is the variance of the Gaussian noise, which controls the perturbation magnitude, and  $\xi^{(n)}$  represents the Gaussian noise sampled at iteration  $n$  to encourage diverse latent trajectories. This strategy introduces controlled exploration in the latent space while preserving the semantic consistency of the original representations, thereby facilitating more effective and robust latent reasoning.

**Entropy-Guided Reward Optimization.** In multimodal anomaly detection, the objective is to identify and localize anomalous regions given a query image along with its cor-

responding textual prompt. Let  $Q = \{q_1, \dots, q_t\}$  denote the sequence of input prompt tokens, and  $I = \{i_1, \dots, i_t\}$  represent the set of visual embeddings extracted from the input image. A MLLM parameterized by  $\theta$  integrates these multimodal inputs to generate a latent reasoning sequence  $\mathcal{G} = \{g_1, \dots, g_N\}$  that supports anomaly detection. The generation process can be formally described using the following autoregressive factorization:

$$\pi_{\theta}(\mathcal{G}|Q, I) = \prod_{n=1}^N \pi_{\theta}(g_n|\mathcal{G}_{<n}, Q, I), \quad (4)$$

where  $\mathcal{G}_{<n}$  denotes the sequence of tokens generated prior to step  $n$ . Accurate reasoning in industrial anomaly detection requires not only reliable predictions but also well-calibrated uncertainty over the model’s internal reasoning states. Existing latent reasoning frameworks typically lack explicit mechanisms to regulate the uncertainty of intermediate representations, potentially resulting in ambiguous or unstable predictions. To address this limitation, we propose an entropy-guided reward mechanism that leverages predictive uncertainty as an intrinsic feedback signal for optimizing latent think tokens. Specifically, for each query instance, we quantify the model’s predictive uncertainty by computing the entropy of its probability distribution as:

$$\mathcal{H}(P_i^{(n)}) = - \sum_{j=1}^C P_i^{(n)}(j) \log P_i^{(n)}(j), \quad (5)$$

where  $P_i^{(n)}$  denotes the predicted probability distribution over answers by the  $i$ -th latent think token at iteration  $n$ . Lower entropy indicates that the model has reached a more confident and deterministic reasoning state, while higher entropy reflects higher epistemic uncertainty arising from unfamiliar or conflicting features. Based on this measure, the global reward at iteration  $n$  is defined as the complement of the mean entropy across all latent think tokens:

$$\mathcal{R}(\mathcal{Z}^{(n)}) = 1 - \frac{1}{m} \sum_{i=1}^m \mathcal{H}(P_i^{(n)}), \quad (6)$$

where higher reward values incentivize the model to reduce uncertainty in its latent reasoning process, thereby encouraging more stable predictions. To iteratively optimize the latent think tokens toward higher confidence (i.e., lower entropy), we adopt a REINFORCE-based policy gradient method (Montenegro et al., 2024). Specifically, given the stochastic perturbations of latent tokens defined in Eq. (3), the update rule at iteration  $n$  is formulated as:

$$\mathcal{Z}'^{(n)} \leftarrow \mathcal{Z}^{(n)} + \eta \nabla_{\mathcal{Z}^{(n)}} J(\mathcal{Z}^{(n)}), \quad (7)$$

where  $\eta$  represents the learning rate, and  $J(\cdot)$  denotes the expected reward objective. Following the Policy Gradient

Table 1. Performance comparison of commercial and open-source MLLMs on the MMAD benchmark under the standard one-shot setting. The best results are highlighted in bold, and all metrics are reported as accuracy (%).

Type	Model	Scale	Anomaly		Defect			Object		Average
			Discrimination	Classification	Localization	Description	Analysis	Classification	Analysis	
Random	Random Chance	-	50.00	25.00	25.00	25.00	25.00	25.00	25.00	28.57
Human	Human (expert)	-	95.24	75.00	92.31	83.33	94.20	86.11	80.37	86.65
	Human (ordinary)	-	86.90	66.25	85.58	71.25	81.52	89.58	69.72	78.69
Commercial	Claude-3.5-sonnet	-	60.14	60.14	48.81	67.13	79.11	85.19	79.83	68.36
	Gemini-2.5-pro	-	83.07	<b>73.86</b>	67.20	<b>79.97</b>	86.27	94.88	83.08	<b>81.19</b>
	Gemini-2.5-flash		<b>83.38</b>	69.88	63.30	76.41	81.57	94.04	82.00	78.65
	GPT-4o	-	68.63	65.80	55.62	73.21	83.41	<b>94.98</b>	82.80	74.92
	GPT-5-mini	-	64.10	67.35	<b>69.07</b>	79.02	<b>86.72</b>	93.96	<b>83.37</b>	77.65
Open Source	Qwen3-VL	2B	70.29	50.42	49.35	64.69	78.09	91.45	80.43	69.24
	Qwen2.5-VL	3B	63.03	47.47	54.87	66.66	80.57	86.85	82.84	68.87
	AnomalyR1	3B	60.62	63.56	<b>70.14</b>	<b>80.47</b>	85.28	92.48	86.15	76.96
	Qwen3-VL	4B	74.02	59.25	62.74	70.09	79.22	92.47	83.59	74.48
	AnomalyGPT	7B	65.57	27.49	27.97	36.86	32.11	29.84	35.82	36.52
	Qwen2.5-VL	7B	71.79	55.23	68.97	64.54	78.90	92.55	84.66	72.38
	LLaVA-1.5	7B	51.33	37.04	36.62	50.60	69.79	68.29	69.53	54.74
	LLaVA-NEXT	7B	57.64	33.79	47.72	51.84	67.93	81.39	74.91	59.32
	LLaVA-OneVision	7B	51.77	46.13	41.85	62.19	69.73	90.31	80.93	63.27
	InternVL2	8B	59.97	43.85	47.91	57.60	78.10	74.18	80.37	63.14
	Qwen3-VL	8B	73.08	62.33	60.34	69.15	80.09	92.53	84.01	74.51
	Qwen3-VL-thinking	8B	52.31	41.50	40.37	45.67	36.02	64.34	53.30	47.64
	GLM-4.1-V-Thinking	9B	72.31	72.01	66.47	79.98	84.61	93.79	83.26	78.92
	LLaVA-1.5	13B	49.96	38.78	46.17	58.17	73.09	73.62	70.98	58.68
	Kimi-VL	16B	66.57	71.72	61.88	79.78	82.93	92.18	<b>86.51</b>	77.37
	LLaVA-NeXT	34B	57.92	48.79	52.87	71.34	80.28	81.12	77.80	67.16
	InternVL2	76B	68.25	54.22	56.66	66.30	80.47	86.40	82.92	70.75
Reason-IAD	Qwen3-VL	2B	61.90	70.20	54.63	71.51	79.92	94.59	81.61	73.48
	Qwen3-VL	4B	75.05	73.72	66.48	76.83	82.33	94.90	84.41	79.10
	Qwen2.5-VL	7B	70.74	67.97	60.82	72.78	82.62	<b>97.17</b>	84.99	76.73
	Qwen3-VL	8B	<b>75.24</b>	<b>75.07</b>	62.78	76.38	<b>85.58</b>	96.31	84.62	<b>79.43</b>

Theorem and considering the Gaussian perturbations, the gradient of the objective can be expressed as:

$$\begin{aligned} \nabla_{\mathcal{Z}} \mathcal{J}(\mathcal{Z}) &= \mathbb{E}_{\mathcal{Z}' \sim \pi(\cdot | \mathcal{Z})} [\mathcal{R}(\mathcal{Z}') \nabla_{\mathcal{Z}} \log \pi(\mathcal{Z}' | \mathcal{Z})] \\ &= \mathbb{E} \left[ \mathcal{R}(\mathcal{Z}') \frac{\xi}{\sigma^2} \right]. \end{aligned} \quad (8)$$

This optimization process encourages the latent tokens to reduce predictive uncertainty, thereby improving the overall reasoning accuracy of the model.

**Dynamic Visual Injection.** Inspired by human cognition, in which uncertain situations often prompt revisiting visual information, we introduce a dynamic visual injection mechanism within the latent reasoning process. This mechanism selectively incorporates the most informative image patches into the latent sequence alongside the latent think tokens, guided by the reward signal at each iteration.

Specifically, we leverage the attention weights of the latent think tokens to identify  $t$  highly relevant image patches. At each iteration, the model resamples  $t$  candidate patches  $V_{cand} = \{v_1, \dots, v_t\}$  according to the attention distribution computed from the current latent sequence, and evaluates their contribution by injecting them into the latent sequence. The optimal patch set  $V_{best}$  is then updated based on the

current reward  $\mathcal{R}$  as follows:

$$V_{best} = \begin{cases} V_{cand}, & \text{if } \mathcal{R} > \mathcal{R}_{best}, \\ V_{best}, & \text{otherwise.} \end{cases} \quad (9)$$

If the current reward  $\mathcal{R}$  exceeds  $\mathcal{R}_{best}$ , the candidate patches are considered to provide more informative visual evidence (e.g., clearer defect patterns or more discriminative local details), and the best patch set  $V_{best}$  is updated accordingly. Otherwise, the previous best patches are retained. As shown in Algorithm 1, through this iterative, reward-guided refinement, the selected visual patches progressively concentrate on regions most relevant to the latent think tokens, thereby guiding the latent reasoning process toward more accurate and efficient anomaly detection.

## 4. Experiments

### 4.1. Experiment Setup

**Compared Baselines.** To comprehensively evaluate the reasoning capabilities of the proposed Reason-IAD, we conduct extensive experiments comparing it against a diverse set of representative models, including both commercial and open-source multimodal large language models (MLLMs) as well as anomaly detection-specific models.

Table 2. Performance comparison of open-source MLLMs on the MMAD benchmark under the standard zero-shot setting. The best results are highlighted in bold, and all metrics are reported as accuracy (%).

Type	Model	Scale	Anomaly		Defect			Object		Average
			Discrimination	Classification	Localization	Description	Analysis	Classification	Analysis	
Open Source	Qwen3-VL	2B	63.27	47.71	52.48	63.48	77.82	92.16	80.03	68.14
	Qwen2.5-VL	3B	60.63	47.03	54.44	63.51	79.25	87.48	82.02	67.77
	Qwen3-VL	4B	65.83	53.97	58.16	66.35	77.82	91.98	83.38	71.07
	Qwen3-VL thinking	4B	64.21	39.61	42.98	48.96	38.32	78.18	64.18	53.78
	Qwen2.5-VL	7B	60.35	49.89	57.51	60.41	75.58	93.39	84.80	68.85
	LLaVA-1.5	7B	50.81	36.82	35.94	50.96	70.45	67.33	69.12	54.49
	InternVL3	8B	64.67	50.91	60.06	65.49	77.16	82.01	83.58	69.13
	Qwen3-VL	8B	67.10	57.98	58.86	66.89	77.65	92.94	83.82	72.18
	Qwen3-VL thinking	8B	63.07	45.81	49.56	53.52	40.63	82.51	66.25	57.34
	LLaVA-NeXT	34B	60.31	51.40	55.47	71.62	80.49	81.45	75.08	67.97
Reason-IAD	Qwen2.5-VL	72B	66.22	57.99	<b>62.95</b>	72.21	81.01	93.92	<b>86.51</b>	74.40
	InternVL2	76B	64.30	51.19	54.20	63.46	79.92	89.34	83.48	69.41
	Qwen3-VL	2B	54.66	68.95	55.28	70.64	79.68	95.28	80.85	72.19
	Qwen3-VL	4B	66.58	70.62	62.82	73.28	<b>80.88</b>	93.80	84.88	76.12
Reason-IAD	Qwen2.5-VL	7B	59.23	61.02	55.39	66.57	78.37	<b>97.36</b>	85.50	71.78
	Qwen3-VL	8B	<b>67.73</b>	<b>73.12</b>	59.74	<b>74.69</b>	80.65	96.78	84.24	<b>76.71</b>

Table 3. Ablation study of different components with Qwen3-VL-8B under the one-shot setting on four public anomaly detection datasets, all metrics are reported as accuracy (%).

Module	Datasets							
	RAKI	EDLR	$V_{patch}$	MVTec	VisA	MVTec-LOCO	GoodsAD	
				85.75	75.44	67.45	69.38	
✓				88.49	77.83	70.76	73.83	
✓	✓			89.52	78.58	71.33	74.69	
✓	✓	✓		<b>89.84</b>	<b>78.93</b>	<b>71.65</b>	<b>75.00</b>	

The commercial baselines include Claude-3.5-Sonnet (Anthropic, 2024), Gemini-2.5-Pro (Comanici et al., 2025), GPT-4o (Hurst et al., 2024), and GPT-5-Mini (Singh et al., 2025). The open-source baselines include Qwen2.5-VL (Bai et al., 2025b), Qwen3-VL (Bai et al., 2025a), LLaVA-1.5 (Liu et al., 2024a), LLaVA-NeXT (Liu et al., 2024b), LLaVA-OneVision (Li et al., 2024a), and InternVL2 (Chen et al., 2024). In addition, we evaluate Reason-IAD against anomaly detection-specific models, including AnomalyGPT (Gu et al., 2024b) and Anomaly-R1 (Chao et al., 2025).

**Benchmarks.** We evaluate Reason-IAD on the MMAD benchmark (Jiang et al., 2024), which assesses performance across seven subtasks: anomaly discrimination, defect classification, defect localization, defect description, defect analysis, object classification, and object analysis. MMAD comprises four datasets: MVTec-AD (Bergmann et al., 2019), VisA (Zou et al., 2022), MVTec-LOCO (Bergmann et al., 2022), and GoodsAD (Zhang et al., 2024).

**Implementation Details.** In this study, we adopt Qwen2.5-VL-7B and Qwen3-VL-2B/4B/8B as the base models. For retrieval, we employ CLIP with a ViT-L/14-336 backbone as the image and text encoders, with top- $k$  set to 2. The number of latent thinking tokens  $\mathcal{Z}$  is set to 4, and the default number of reasoning iterations is 10. The learning rate is fixed at

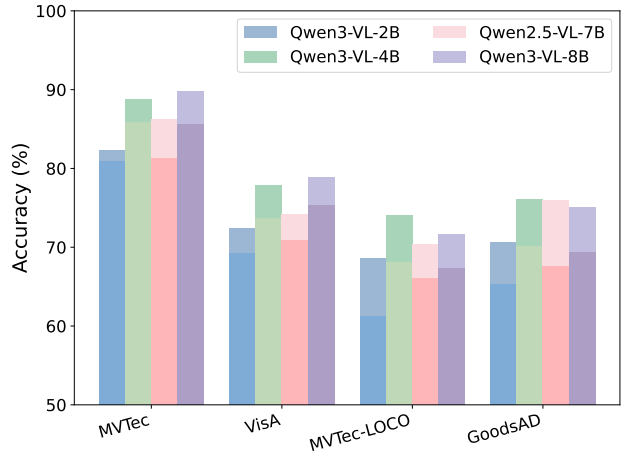


Figure 3. Performance gains of Reason-IAD over baseline models under the one-shot setting.

$1 \times 10^{-3}$ . To ensure stable exploration in the latent space, we set the perturbation magnitude to 10%. By default, we employ a one-shot setting with a randomly sampled normal image from the same domain as the reference template. For comparison, we also evaluate a zero-shot setting. All experiments are conducted on four NVIDIA A100 GPUs (80GB). More details are provided in the Appendix.

## 4.2. Main Results

Table 1 compares Reason-IAD with state-of-the-art methods under the one-shot setting. Reason-IAD consistently demonstrates strong performance across all seven tasks. On Qwen3-VL-8B, it achieves an average accuracy of 79.73%, improving 4.92% over the base model, and even surpasses the commercial model Chat-GPT-4O, which achieves 74.92%. Although designed for anomaly detection, AnomalyGPT underperforms on classification and localization

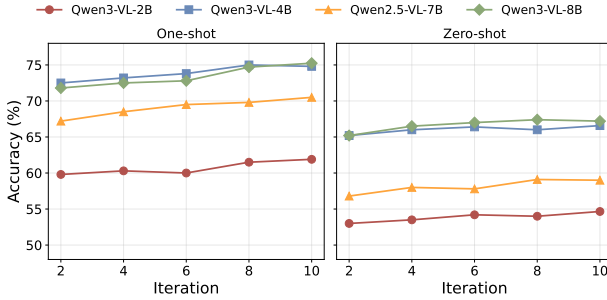


Figure 4. Effect of iteration count on anomaly discrimination performance. Increasing iterations consistently improves accuracy while maintaining stability.

tasks, which may be attributed to catastrophic forgetting when MLLMs are trained on expert outputs. Another domain-specific method, AnomalyR1, incorporates GRPO to further enhance anomaly understanding. In contrast, our training-free approach still outperforms AnomalyR1 by 2.43% in average accuracy, demonstrating that our multimodal reasoning strategy provides more precise anomaly detection and superior image analysis. Notably, Reason-IAD surpasses standard human annotators on defect analysis and object classification tasks. Furthermore, while Qwen3-VL-thinking relies on explicit reasoning chains that generate lengthy intermediate outputs, our implicit reasoning achieves a 31.79% gain in performance, highlighting the effectiveness and efficiency of Reason-IAD.

Table 2 presents zero-shot results. Even without reference images, Reason-IAD substantially improves base models, with Qwen3-4B/8B achieving average accuracy gains of 5.05% and 4.53%, respectively. Notably, our 8B model outperforms InternVL2-76B by 7.30%, further demonstrating the effectiveness of Reason-IAD in anomaly understanding.

### 4.3. Model Analysis

**Ablation Study.** To evaluate the contributions of key components in the proposed Reason-IAD, we conduct ablation studies on four public datasets, as summarized in Table 3. Incorporating knowledge guidance consistently improves detection accuracy across all datasets. Specifically, on MVTec, accuracy increases from 85.75% to 88.49%, with an average gain of 3.22% across the four datasets, highlighting the critical role of prior knowledge. Latent reasoning further enhances performance by 1.03%, improving the model’s inference capability. Moreover, integrating visual information provides an additional average improvement of 0.33%, indicating that the model effectively leverages visual evidence during reasoning. When all components are combined, Reason-IAD achieves the best overall performance, underscoring the effectiveness of the proposed modules.

**Performance Gain of Reason-IAD.** To more intuitively

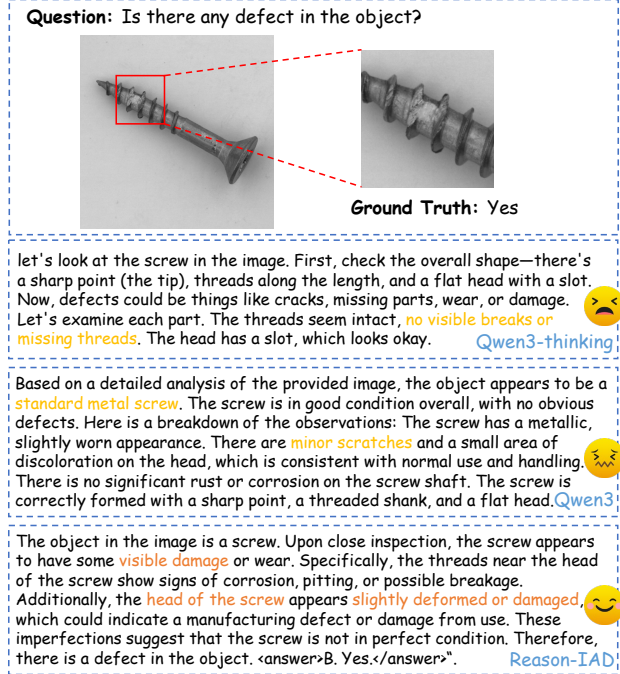


Figure 5. Comparison of model outputs for anomaly detection.

demonstrate the improvements brought by Reason-IAD, we measure its performance gains over the baseline models. As shown in Figure 3, Reason-IAD consistently outperforms all four base models. The improvement is particularly pronounced on the GoodsAD dataset, with an average gain of 6.27%, and remains substantial on the more challenging VisA dataset, with a 3.51% gain, attributable to the effective integration of knowledge guidance and latent reasoning.

**Impact of Iteration Number.** To evaluate the effect of iteration count on model performance, we conduct experiments on four base models for anomaly detection, as shown in Figure 4. The results indicate that increasing the number of iterations consistently improves anomaly reasoning, demonstrating that iterative optimization effectively enhances latent reasoning. Although minor fluctuations occur in intermediate steps, the models maintain high accuracy and continue to benefit from additional iterations, highlighting their capacity to leverage iterative optimization. Iterations are fixed at 10 to balance performance and efficiency.

**Qualitative Analysis.** Figure 5 presents the outputs of various models on the anomaly detection task. Both Qwen3-thinking and Qwen3 fail to produce accurate predictions. Although Qwen3 detects some potential defects, it ultimately misclassifies the image as normal. In contrast, Reason-IAD generates the correct prediction while accurately identifying the key visual evidence of fine-grained industrial defects.

## 5. Conclusion

In this work, we introduce Reason-IAD, a knowledge-guided dynamic latent reasoning framework for explainable industrial anomaly detection. By integrating a retrieval-augmented knowledge module, an entropy-driven latent reasoning mechanism, and a dynamic visual injection strategy, Reason-IAD facilitates context-aware, iterative reasoning over fine-grained industrial defects while effectively leveraging critical visual evidence. Extensive experiments on multiple datasets demonstrate that Reason-IAD consistently outperforms state-of-the-art methods, achieving both high detection accuracy and interpretable reasoning. In summary, Reason-IAD provides a promising paradigm for training-free, expert-level anomaly detection. Future directions include adaptive knowledge retrieval and advanced latent optimization strategies to further enhance the applicability of MLLMs across diverse industrial scenarios.

## Impact Statement

This paper presents work whose goal is to advance the field of Machine Learning, particularly in explainable industrial anomaly detection. The proposed Reason-IAD framework integrates retrieval-augmented knowledge with entropy-driven latent reasoning and dynamic visual injection to address the challenge of fine-grained defect identification and interpretable reasoning. Following this direction, the framework is broadly applicable to other industrial and quality-control settings that require precise anomaly detection and explainable model decisions. There are many potential societal consequences of our work, none of which we feel must be specifically highlighted here.

## References

Amizadeh, S., Palangi, H., Polozov, A., Huang, Y., and Koishida, K. Neuro-symbolic visual reasoning: Disentangling. In *International Conference on Machine Learning*, pp. 279–290. Pmlr, 2020.

Anthropic. Claude 3 model family: Opus, sonnet, haiku. <https://www.anthropic.com>, 2024. Model card for Claude-3 series.

Bai, S., Cai, Y., Chen, R., Chen, K., Chen, X., Cheng, Z., Deng, L., Ding, W., Gao, C., Ge, C., Ge, W., Guo, Z., Huang, Q., Huang, J., Huang, F., Hui, B., Jiang, S., Li, Z., Li, M., Li, M., Li, K., Lin, Z., Lin, J., Liu, X., Liu, J., Liu, C., Liu, Y., Liu, D., Liu, S., Lu, D., Luo, R., Lv, C., Men, R., Meng, L., Ren, X., Ren, X., Song, S., Sun, Y., Tang, J., Tu, J., Wan, J., Wang, P., Wang, P., Wang, Q., Wang, Y., Xie, T., Xu, Y., Xu, H., Xu, J., Yang, Z., Yang, M., Yang, J., Yang, A., Yu, B., Zhang, F., Zhang, H., Zhang, X., Zheng, B., Zhong, H., Zhou, J., Zhou, F., Zhou, J., Zhu, Y., and Zhu, K. Qwen3-v1 technical report, 2025a. URL <https://arxiv.org/abs/2511.21631>.

Bai, S., Chen, K., Liu, X., Wang, J., Ge, W., Song, S., Dang, K., Wang, P., Wang, S., Tang, J., et al. Qwen2.5-v1 technical report. *arXiv preprint arXiv:2502.13923*, 2025b.

Bergmann, P., Fauser, M., Sattlegger, D., and Steger, C. Mvtac ad—a comprehensive real-world dataset for unsupervised anomaly detection. In *Proceedings of the IEEE/CVF conference on computer vision and pattern recognition*, pp. 9592–9600, 2019.

Bergmann, P., Batzner, K., Fauser, M., Sattlegger, D., and Steger, C. Beyond dents and scratches: Logical constraints in unsupervised anomaly detection and localization. *International Journal of Computer Vision*, 130(4): 947–969, 2022.

Cao, Y., Zhang, J., Frittoli, L., Cheng, Y., Shen, W., and Bozicchi, G. Adaclip: Adapting clip with hybrid learnable prompts for zero-shot anomaly detection. In *European Conference on Computer Vision*, pp. 55–72. Springer, 2024.

Chao, Y., Liu, J., Tang, J., and Wu, G. Anomalyr1: A group-based end-to-end mllm for industrial anomaly detection. *arXiv preprint arXiv:2504.11914*, 2025.

Chen, P., He, W., Qian, F., Shi, G., and Yan, J. A synergistic cnn-transformer network with pooling attention fusion for hyperspectral image classification. *Digital Signal Processing*, 160:105070, 2025a.

Chen, P., Huang, F., and Huang, C. Dyc-clip: Dynamic context-aware multi-modal prompt learning for zero-shot anomaly detection. *Pattern Recognition*, pp. 113215, 2026.

Chen, X., Zhao, A., Xia, H., Lu, X., Wang, H., Chen, Y., Zhang, W., Wang, J., Li, W., and Shen, X. Reasoning beyond language: A comprehensive survey on latent chain-of-thought reasoning. *arXiv preprint arXiv:2505.16782*, 2025b.

Chen, Z., Wu, J., Wang, W., Su, W., Chen, G., Xing, S., Zhong, M., Zhang, Q., Zhu, X., Lu, L., et al. Internvl: Scaling up vision foundation models and aligning for generic visual-linguistic tasks. In *Proceedings of the IEEE/CVF conference on computer vision and pattern recognition*, pp. 24185–24198, 2024.

Comanici, G., Bieber, E., Schaekermann, M., Pasupat, I., Sachdeva, N., Dhillon, I., Blistein, M., Ram, O., Zhang, D., Rosen, E., et al. Gemini 2.5: Pushing the frontier with advanced reasoning, multimodality, long context, and next generation agentic capabilities. *arXiv preprint arXiv:2507.06261*, 2025.

Deng, H. and Li, X. Anomaly detection via reverse distillation from one-class embedding. In *Proceedings of the IEEE/CVF conference on computer vision and pattern recognition*, pp. 9737–9746, 2022.

Ding, Y. and Zhang, R. Sherlock: Self-correcting reasoning in vision-language models. *arXiv preprint arXiv:2505.22651*, 2025.

Fang, Y., Fang, Y., Chen, R., Xu, H., Ding, X., and Huang, Y. Demeaned sparse: Efficient anomaly detection by residual estimate. In *Forty-second International Conference on Machine Learning*, 2024.

Feng, Y., Chen, W., Li, Y., Chen, B., Wang, Y., Zhao, Z., Liu, H., and Zhou, M. Omiad: One-step adaptive masked diffusion model for multi-class anomaly detection via adversarial distillation. In *Proceedings of the 42nd International Conference on Machine Learning*, pp. 16604–16633, 2025.

Geiping, J., McLeish, S., Jain, N., Kirchenbauer, J., Singh, S., Bartoldson, B. R., Kailkhura, B., Bhatele, A., and Goldstein, T. Scaling up test-time compute with latent reasoning: A recurrent depth approach. *arXiv preprint arXiv:2502.05171*, 2025.

Gu, Z., Zhu, B., Zhu, G., Chen, Y., Li, H., Tang, M., and Wang, J. Filo: Zero-shot anomaly detection by fine-grained description and high-quality localization. In *Proceedings of the 32nd ACM International Conference on Multimedia*, pp. 2041–2049, 2024a.

Gu, Z., Zhu, B., Zhu, G., Chen, Y., Tang, M., and Wang, J. Anomalygpt: Detecting industrial anomalies using large vision-language models. In *Proceedings of the AAAI conference on artificial intelligence*, volume 38, pp. 1932–1940, 2024b.

Gupta, T. and Kembhavi, A. Visual programming: Compositional visual reasoning without training. In *Proceedings of the IEEE/CVF conference on computer vision and pattern recognition*, pp. 14953–14962, 2023.

Hao, S., Sukhbaatar, S., Su, D., Li, X., Hu, Z., Weston, J., and Tian, Y. Training large language models to reason in a continuous latent space. *arXiv preprint arXiv:2412.06769*, 2024.

Huang, C.-P., Wu, Y.-H., Chen, M.-H., Wang, Y.-C. F., and Yang, F.-E. Thinkact: Vision-language-action reasoning via reinforced visual latent planning. *arXiv preprint arXiv:2507.16815*, 2025.

Hurst, A., Lerer, A., Goucher, A. P., Perelman, A., Ramesh, A., Clark, A., Ostrow, A., Welihinda, A., Hayes, A., Radford, A., et al. Gpt-4o system card. *arXiv preprint arXiv:2410.21276*, 2024.

Jeong, J., Zou, Y., Kim, T., Zhang, D., Ravichandran, A., and Dabeer, O. Winclip: Zero-/few-shot anomaly classification and segmentation. In *Proceedings of the IEEE/CVF Conference on Computer Vision and Pattern Recognition*, pp. 19606–19616, 2023.

Jiang, X., Li, J., Deng, H., Liu, Y., Gao, B.-B., Zhou, Y., Li, J., Wang, C., and Zheng, F. Mmad: A comprehensive benchmark for multimodal large language models in industrial anomaly detection. *arXiv preprint arXiv:2410.09453*, 2024.

Li, B., Zhang, Y., Guo, D., Zhang, R., Li, F., Zhang, H., Zhang, K., Zhang, P., Li, Y., Liu, Z., et al. Llava-onevision: Easy visual task transfer. *arXiv preprint arXiv:2408.03326*, 2024a.

Li, B., Sun, X., Liu, J., Wang, Z., Wu, J., Yu, X., Chen, H., Barsoum, E., Chen, M., and Liu, Z. Latent visual reasoning. *arXiv preprint arXiv:2509.24251*, 2025a.

Li, H., Li, C., Wu, T., Zhu, X., Wang, Y., Yu, Z., Jiang, E. H., Zhu, S.-C., Jia, Z., Wu, Y. N., et al. Seek in the dark: Reasoning via test-time instance-level policy gradient in latent space. *arXiv preprint arXiv:2505.13308*, 2025b.

Li, X., Zhang, Z., Tan, X., Chen, C., Qu, Y., Xie, Y., and Ma, L. Promptad: Learning prompts with only normal samples for few-shot anomaly detection. In *Proceedings of the IEEE/CVF Conference on Computer Vision and Pattern Recognition*, pp. 16838–16848, 2024b.

Li, Y., Cao, Y., Liu, C., Xiong, Y., Dong, X., and Huang, C. Iad-r1: Reinforcing consistent reasoning in industrial anomaly detection. *arXiv preprint arXiv:2508.09178*, 2025c.

Li, Y., Yuan, S., Wang, H., Li, Q., Liu, M., Xu, C., Shi, G., and Zuo, W. Triad: Empowering lmm-based anomaly detection with expert-guided region-of-interest tokenizer and manufacturing process. In *Proceedings of the IEEE/CVF International Conference on Computer Vision*, pp. 21917–21926, 2025d.

Liao, J., Su, Y., Tu, R.-C., Jin, Z., Sun, W., Li, Y., Tao, D., Xu, X., and Yang, X. Ad-fm: Multimodal llms for anomaly detection via multi-stage reasoning and fine-grained reward optimization. *arXiv preprint arXiv:2508.04175*, 2025.

Liu, C., Yang, Y., Fan, Y., Wei, Q., Liu, S., and Wang, X. E. Reasoning within the mind: Dynamic multimodal interleaving in latent space. *arXiv preprint arXiv:2512.12623*, 2025.

Liu, H., Li, C., Li, Y., and Lee, Y. J. Improved baselines with visual instruction tuning. In *Proceedings of the IEEE/CVF conference on computer vision and pattern recognition*, pp. 26296–26306, 2024a.

Liu, H., Li, C., Li, Y., Li, B., Zhang, Y., Shen, S., and Lee, Y. J. Llava-next: Improved reasoning, ocr, and world knowledge, january 2024. *URL* <https://llava-vl.github.io/blog/2024-01-30-llava-next>, 1(8), 2024b.

Ma, W., Zhang, X., Yao, Q., Tang, F., Wu, C., Li, Y., Yan, R., Jiang, Z., and Zhou, S. K. Aa-clip: Enhancing zero-shot anomaly detection via anomaly-aware clip. In *Proceedings of the Computer Vision and Pattern Recognition Conference*, pp. 4744–4754, 2025.

Montenegro, A., Mussi, M., Papini, M., and Metelli, A. M. Last-iterate global convergence of policy gradients for constrained reinforcement learning. *Advances in Neural Information Processing Systems*, 37:126363–126416, 2024.

Pham, T.-H. and Ngo, C. Multimodal chain of continuous thought for latent-space reasoning in vision-language models. *arXiv preprint arXiv:2508.12587*, 2025.

Qu, Z., Tao, X., Prasad, M., Shen, F., Zhang, Z., Gong, X., and Ding, G. Vcp-clip: A visual context prompting model for zero-shot anomaly segmentation. In *European Conference on Computer Vision*, pp. 301–317. Springer, 2024.

Qu, Z., Tao, X., Gong, X., Qu, S., Chen, Q., Zhang, Z., Wang, X., and Ding, G. Bayesian prompt flow learning for zero-shot anomaly detection. In *Proceedings of the Computer Vision and Pattern Recognition Conference*, pp. 30398–30408, 2025.

Radford, A., Kim, J. W., Hallacy, C., Ramesh, A., Goh, G., Agarwal, S., Sastry, G., Askell, A., Mishkin, P., Clark, J., et al. Learning transferable visual models from natural language supervision. In *International conference on machine learning*, pp. 8748–8763. PMLR, 2021.

Roth, K., Pemula, L., Zepeda, J., Schölkopf, B., Brox, T., and Gehler, P. Towards total recall in industrial anomaly detection. In *Proceedings of the IEEE/CVF conference on computer vision and pattern recognition*, pp. 14318–14328, 2022.

Ruan, Y., Band, N., Maddison, C. J., and Hashimoto, T. Reasoning to learn from latent thoughts. *arXiv preprint arXiv:2503.18866*, 2025.

Shi, Y., Li, S., Wu, C., Liu, Z., Fang, J., Cai, H., Zhang, A., and Wang, X. Search and refine during think: Facilitating knowledge refinement for improved retrieval-augmented reasoning. In *The Thirty-ninth Annual Conference on Neural Information Processing Systems*, 2025.

Singh, A., Fry, A., Perelman, A., Tart, A., Ganesh, A., El-Kishky, A., McLaughlin, A., Low, A., Ostrow, A., Ananthram, A., et al. Openai gpt-5 system card. *arXiv preprint arXiv:2601.03267*, 2025.

Sun, G., Hua, H., Wang, J., Luo, J., Dianat, S., Rabbani, M., Rao, R., and Tao, Z. Latent chain-of-thought for visual reasoning. *arXiv preprint arXiv:2510.23925*, 2025.

Tan, H., Ji, Y., Hao, X., Chen, X., Wang, P., Wang, Z., and Zhang, S. Reason-rft: Reinforcement fine-tuning for visual reasoning of vision language models. In *The Thirty-ninth Annual Conference on Neural Information Processing Systems*, 2025a.

Tan, W., Li, J., Ju, J., Luo, Z., Luan, J., and Song, R. Think silently, think fast: Dynamic latent compression of llm reasoning chains. *arXiv preprint arXiv:2505.16552*, 2025b.

Wan, Z., Dou, Z., Liu, C., Zhang, Y., Cui, D., Zhao, Q., Shen, H., Xiong, J., Xin, Y., Jiang, Y., et al. Srpo: Enhancing multimodal llm reasoning via reflection-aware reinforcement learning. *arXiv preprint arXiv:2506.01713*, 2025.

Wang, H., Qu, C., Huang, Z., Chu, W., Lin, F., and Chen, W. Vl-rethinker: Incentivizing self-reflection of vision-language models with reinforcement learning. *arXiv preprint arXiv:2504.08837*, 2025a.

Wang, X., Wang, X., Bai, H., Lim, E. G., and Xiao, J. Cnc: Cross-modal normality constraint for unsupervised multi-class anomaly detection. In *Proceedings of the AAAI Conference on Artificial Intelligence*, volume 39, pp. 7943–7951, 2025b.

Xu, J., Lo, S.-Y., Safaei, B., Patel, V. M., and Dwivedi, I. Towards zero-shot anomaly detection and reasoning with multimodal large language models. In *Proceedings of the Computer Vision and Pattern Recognition Conference*, pp. 20370–20382, 2025.

Yan, F., Jiang, X., Lu, Y., Cao, J., Chen, D., and Xu, M. Wavelet and prototype augmented query-based transformer for pixel-level surface defect detection. In *Proceedings of the Computer Vision and Pattern Recognition Conference*, pp. 23860–23869, 2025.

Yang, Z., Yu, X., Chen, D., Shen, M., and Gan, C. Machine mental imagery: Empower multimodal reasoning with latent visual tokens. *arXiv preprint arXiv:2506.17218*, 2025.

Zhang, J., Ding, R., Ban, M., and Dai, L. Pku-goodsad: A supermarket goods dataset for unsupervised anomaly detection and segmentation. *IEEE Robotics and Automation Letters*, 9(3):2008–2015, 2024.

Zhang, J., Wang, G., Jin, Y., and Huang, D. Towards training-free anomaly detection with vision and language foundation models. In *Proceedings of the Computer Vision and Pattern Recognition Conference*, pp. 15204–15213, 2025a.

Zhang, Q., Shao, M., Chen, X., Lv, X., and Xu, K. Wave-mambaad: Wavelet-driven state space model for multi-class unsupervised anomaly detection. In *Proceedings of the IEEE/CVF International Conference on Computer Vision*, pp. 20868–20877, 2025b.

Zhang, Z., He, X., Yan, W., Shen, A., Zhao, C., Wang, S., Shen, Y., and Wang, X. E. Soft thinking: Unlocking the reasoning potential of llms in continuous concept space. *arXiv preprint arXiv:2505.15778*, 2025c.

Zhou, Q., Pang, G., Tian, Y., He, S., and Chen, J. Anomalyclip: Object-agnostic prompt learning for zero-shot anomaly detection. *arXiv preprint arXiv:2310.18961*, 2023.

Zou, Y., Jeong, J., Pemula, L., Zhang, D., and Dabeer, O. Spot-the-difference self-supervised pre-training for anomaly detection and segmentation. In *European conference on computer vision*, pp. 392–408. Springer, 2022.

## Appendix.

### A. More Details about Evaluation

#### A.1. Experiment Setup.

To comprehensively evaluate the reasoning capabilities of the proposed Reason-IAD, we conduct extensive experiments comparing it against a diverse set of representative models. These include both commercial and open-source multimodal large language models (MLLMs), as well as models specifically designed for anomaly detection. The commercial baselines include Claude-3.5-Sonnet (Anthropic, 2024), Gemini-2.5-Pro (Comanici et al., 2025), GPT-4o (Hurst et al., 2024), and GPT-5-Mini (Singh et al., 2025). The open-source baselines include Qwen2.5-VL (Bai et al., 2025b), Qwen3-VL (Bai et al., 2025a), LLaVA-1.5 (Liu et al., 2024a), LLaVA-NeXT (Liu et al., 2024b), LLaVA-OneVision (Li et al., 2024a), and InternVL2 (Chen et al., 2024). In addition, we benchmark Reason-IAD against anomaly detection-specific models, such as AnomalyGPT (Gu et al., 2024b) and Anomaly-R1 (Chao et al., 2025), to evaluate its performance relative to domain-specialized approaches.

For our experiments, we use Qwen2.5-VL-7B and Qwen3-VL-2B/4B/8B as base models. In the retrieval stage, we employ the CLIP model with a ViT-L/14-336 backbone as the image and text encoder, with top- $k$  set to 2. The number of latent thinking tokens  $\mathcal{Z}$  is set to 4, and the default number of reasoning iterations is 10. The learning rate is fixed at  $1 \times 10^{-3}$ , and the perturbation magnitude is set to 10% to ensure stable exploration in the latent space. By default, we adopt a one-shot setting, where a normal image from the same domain is randomly sampled as a reference template to help the model capture the normal appearance of objects. For comparison, we also evaluate the models under a zero-shot setting, which tests their ability to perform pairwise comparisons between industrial images without reference guidance. This evaluation protocol provides a comprehensive assessment of the models' reasoning capabilities in both reference-based and reference-free scenarios. All experiments are conducted on four NVIDIA A100 GPUs (80GB).

#### A.2. Datasets.

Table 4. Statistics on the composition and quantity of test data.

Image Source	Sampled Images	Generated Questions	Object Categories	Defect Categories
MVTec-AD (Bergmann et al., 2019)	1691	8338	15	73
MVTec-LOCO-AD (Bergmann et al., 2022)	1566	7624	5	89
VisA (Zou et al., 2022)	2141	10622	12	67
GoodsAD (Zhang et al., 2024)	2968	13088	6	15
<b>SUM</b>	<b>8366</b>	<b>39672</b>	<b>38</b>	<b>244</b>

We evaluate Reason-IAD on multiple industrial anomaly detection (IAD) datasets with diverse characteristics, covering over 38 product categories and 244 defect types, as summarized in Table 4. Among these, MVTec AD is one of the most widely used benchmarks for IAD, encompassing a variety of object and texture categories; we further leverage fine-grained annotations from Defect Spectrum to provide more detailed defect descriptions. MVTec LOCO AD focuses on logical anomalies, thereby evaluating the model's ability to reason about high-level logical inconsistencies. The VisA dataset contains multiple instances with complex defect patterns, reflecting more challenging real-world IAD scenarios. GoodsAD primarily consists of industrial goods, and due to the diverse appearances of finished products across different brands, it significantly increases the number of object categories and visual variations.

In our experiments, we adopt the MMAD benchmark as the evaluation protocol, which comprises seven subtasks: (1) Anomaly Discrimination Detection, a binary classification task that determines whether a sample is defective, to evaluate the model's fundamental anomaly detection capability; (2) Defect Classification, which identifies the specific defect type, jointly assessing anomaly recognition and domain knowledge of industrial defect categories; (3) Defect Localization, requiring the model to locate defective regions, where standardized textual descriptions are used instead of explicit segmentation masks; (4) Defect Description, which characterizes defect attributes (e.g., size and color), simulating practical defect inspection scenarios; (5) Defect Analysis, analyzing the potential impact of defects on product quality to estimate their severity; (6) Object Classification, categorizing industrial products to facilitate anomaly detection based on an understanding of normal object characteristics; and (7) Object Analysis, querying the composition, position, and function of products to evaluate fine-grained semantic understanding.

Table 5. Performance comparison of different MLLMs in Anomaly Discrimination Tasks.

	Model	Scale	Accuracy	Recall	Precision	F1
Human	Human (expert)	-	95.24	94.25	98.89	96.43
	Human (ordinary)	-	86.90	87.07	94.35	89.30
Commercial	claude-3.5-sonnet	-	60.14	30.87	76.75	41.92
	Gemini-1.5-flash	-	58.58	78.63	67.41	72.40
	Gemini-1.5-pro	-	68.63	45.47	86.84	57.60
	GPT-4o-mini	-	64.33	65.47	73.04	68.67
	GPT-4o	-	68.63	67.37	75.68	71.04
	Qwen3-VL	2B	69.24	66.83	79.78	71.64
Open Source	Qwen3-VL	4B	74.48	57.95	89.41	67.01
	AnomalyGPT	7B	65.57	82.11	74.45	76.68
	Qwen2.5-VL	7B	68.87	53.74	75.54	61.48
	Qwen-VL-Chat	7B	53.65	43.95	65.39	47.28
	LLaVA-1.5	7B	51.33	94.79	62.72	75.32
	Qwen3-VL	8B	74.51	75.58	79.76	77.43
	Cambrian-1*	8B	55.60	22.28	74.10	31.85
	SPHINX*	7B	53.13	6.42	99.74	10.61
	LLaVA-NEXT-Interleave	7B	57.64	16.58	90.83	25.64
	InternLM-XComposer2-VL	7B	55.85	17.94	75.87	27.16
	LLaVA-OnVision	7B	51.77	4.90	78.19	9.10
	MiniCPM-V2.6	8B	57.31	34.38	70.98	45.31
	InternVL2	8B	59.97	30.25	79.22	41.23
Reason-IAD	LLaVA-1.5	13B	49.96	99.79	62.00	76.28
	LLaVA-NeXT	34B	57.92	46.27	69.98	54.44
	InternVL2	76B	68.25	55.81	83.52	64.40
	Qwen3-VL	2B	73.48	92.23	69.19	78.75
Reason-IAD	Qwen3-VL	4B	79.20	68.21	86.40	75.49
	Qwen2.5-VL	7B	73.91	55.50	75.95	62.15
	Qwen3-VL	8B	79.42	73.77	83.37	73.08

### A.3. Prompt Design

To guide the multimodal large language models (MLLMs) to perform domain-specific anomaly reasoning, we design a structured prompt that explicitly defines the model as an industrial inspection expert and incorporates category-level domain knowledge. Specifically, the prompt instructs the model to determine whether the queried image contains defects and to answer the associated questions based on visual evidence. To encourage reliable decision-making, the model is required to perform internal reasoning before producing the final prediction.

Moreover, we inject retrieved domain knowledge describing typical defect types and normal object characteristics into the prompt, enabling context-aware reasoning tailored to industrial scenarios. This design allows the model to leverage both visual observations and prior knowledge, facilitating accurate and interpretable anomaly detection. The prompt template is defined as follows:

You are an expert industrial inspector responsible for analyzing product images. Your task is to determine whether the query image contains any defects and to answer the related questions. You should first perform the reasoning process internally and then provide the final answer. The following domain knowledge describes typical defect types and normal object characteristics: \n {Domain\_knowledge}.

### A.4. Additional Experimental Results.

To comprehensively evaluate model performance on the anomaly discrimination task, we adopt the standard anomaly detection setup, treating anomalous samples as the positive class and normal samples as the negative class, reporting recall, precision, and F1-score. As shown in Table 5, analysis of recall and precision highlights the reasons for suboptimal

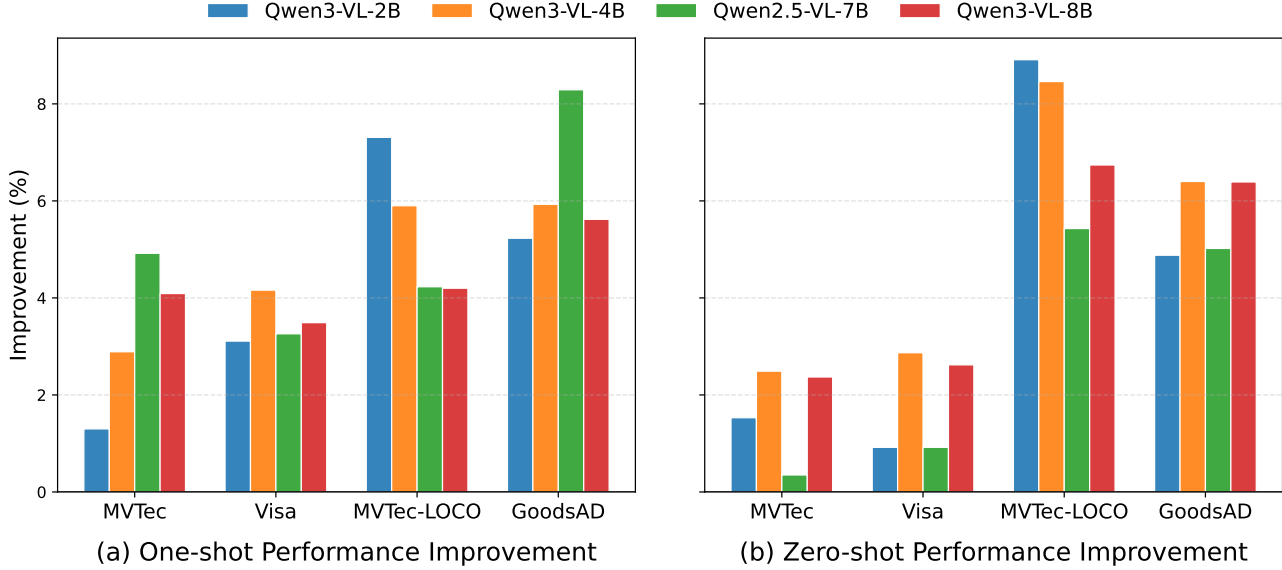


Figure 6. Performance gains of Reason-IAD over baseline models under the one-shot and zero-shot setting.

performance in certain models. For example, both SPHINX and LLaVAOnVision frequently misclassify anomalies as normal, leading to many missed detections, while LLaVA-1.5 shows high recall but low precision, reflecting a substantial false positive rate. Human experts outperform all MLLMs, with experts achieving over 94% across metrics and ordinary individuals over 87%. Notably, AnomalyGPT, specifically trained for anomaly detection, outperforms most models but still exhibits a significant false positive issue. Our proposed Reason-IAD effectively mitigates these limitations, enhancing detection performance by leveraging knowledge priors and a latent reasoning strategy. Moreover, the accuracy of all four models exceeds 73%.

As shown in Figure 6, consistent performance gains are observed under both one-shot and zero-shot settings. Compared with the baseline models, the proposed Reason strategy consistently achieves notable gains across all backbones. In the one-shot setting, the largest improvement is observed on the GoodsAD dataset with Qwen2.5-VL-7B, reaching 8.29%, followed by Qwen3-VL-2B, which achieves a gain of 7.31% on MVTec-LOCO. In the zero-shot setting, Qwen3-VL-2B and Qwen3-VL-4B obtain improvements of 8.91% and 8.46% on the MVTec dataset, respectively. These results demonstrate that the proposed reasoning strategy significantly enhances anomaly detection performance across different model scales and evaluation settings, indicating strong robustness and generalization capability.

## B. Case Study

As shown in Figures 7–14, we further present several qualitative case studies on representative industrial anomaly detection scenarios featuring diverse defect patterns and object categories. These examples are provided to visually demonstrate the effectiveness of the proposed Reason-IAD in identifying anomalous regions, as well as its interpretability in explaining the underlying defect characteristics through structured reasoning.

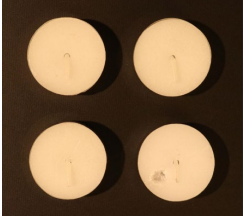


 **Question:**  
Is there any defect in the object?  
A. No.    B. Yes.

**Answer:**

The object in the image is a hazelnut. Upon close inspection, there is a noticeable hole or indentation on the surface of the nut, particularly visible on the right side. This appears to be a physical defect, possibly caused by insect damage, a natural blemish, or a break in the shell. Since the question asks whether there is any defect, and a clear imperfection is visible, the correct answer is that there is a defect. 

Figure 7. A case study of the anomaly discrimination task on the MVTec-AD dataset.



 **Question:**  
There is a defect in the object. Where is the defect?  
A. Top left candle    B. Bottom right candle  
C. Bottom left candle    D. Top right

**Answer:**

Looking at the image, I need to find which candle has a defect. I am examining each candle one by one: Top left candle: appears normal, wick is intact. Top right candle: appears normal, wick is intact. Bottom left candle: appears normal, wick is intact. Bottom right candle: I can see a small, dark, smudged area near the wick, which looks like a burn mark or a defect from previous use. This defect is clearly visible on the bottom right candle. 

Figure 8. A case study of the defect location task on the Visa dataset.



 **Question:**  
Is there any defect in the object?  
A. Yes.    B. No.

**Answer:**

The object in the image is a screw. Upon close inspection, the head of the screw shows visible damage or wear, particularly around the slot where a driver would be inserted. The slot appears chipped or broken, which would prevent a standard screwdriver from engaging properly. This is a clear defect that compromises the functionality of the screw. 

Figure 9. A case study of the anomaly discrimination task on the MVTec-AD dataset.



**Question:**

There is a defect in the object. Where is the defect?

A. Top right. B. Bottom right.  
C. Center left. D. Center.



**Answer:**

Looking at the image, I need to find where the defect is located. The image shows a brown leather-like surface with a characteristic grain pattern. I need to scan the entire image to locate any imperfections. Scanning the image: The top right area appears to have the normal leather texture. The bottom right area also appears normal. The center area has the typical grain pattern. Looking at the center left area, I can see a small, dark, irregular spot that breaks the uniformity of the leather texture. This appears to be a small hole or tear in the material. This defect is located in the center left portion of the image. **C. Center left.**



Figure 10. A case study of the defect location task on the Visa dataset.



**Question:**

There is a defect in the object. What is the appearance of the defect?

A. Peeling paint B. Circular stain  
C. Vertical indent D. Horizontal scratch

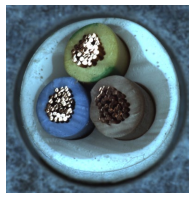


**Answer:**

Looking at the image of the Coca-Cola can, I can see a clear defect on the red surface. There is a noticeable white mark running vertically along the side of the can, interrupting the red background. This mark appears to be a scratch or scuff, not a stain, hole, or faded area. It is elongated and follows a vertical path, which matches option B. **B. A vertical scratch or scuff.**



Figure 11. A case study of the defect description task on the GoodsAD dataset.



**Question:**

What kind of product is in the image?

A. Rubber hose. B. Three-core electrical cable.  
C. Plumbing pipe. D. Fiber optic cable.



**Answer:**

The image shows a cross-section of a cable with three distinct inner conductors, each surrounded by insulation. The conductors appear to be made of copper (shiny, metallic strands), which is typical for electrical wiring. The outer layer is a white sheath, likely for protection and bundling. This structure is characteristic of a multi-core electrical cable used for transmitting electrical power or signals. The presence of three insulated copper conductors strongly indicates a three-core electrical cable, commonly used in electrical installations. **B. Three-core electrical cable.**



Figure 12. A case study of the object classification task on the MVTec-AD dataset.



**Question:**

There is a defect in the object. What is the appearance of the defect?

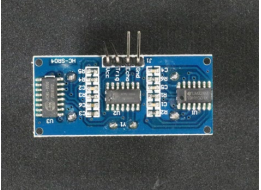
A. The bottle is dented  
 B. The label is peeling off  
 C. The cap is slightly ajar on one side  
 D. The cap is completely missing

**Answer:**

Looking at the image, I need to carefully examine the bottle for any defects among the given options. I can see the bottle is standing upright and appears to have a normal, smooth shape without any visible dents or deformations. The label appears to be intact and fully adhered to the bottle. There are no signs of peeling or lifting at any point. Looking closely at the cap, it appears to be securely closed. There is no visible gap or misalignment on any side. The cap is clearly present on top of the bottle. After carefully examining all aspects of the bottle, I can see that there is no defect present among the listed options. The bottle appears to be in perfect condition. Upon closer inspection, I notice that the cap appears to be slightly misaligned or not perfectly seated, which could be interpreted as \"slightly ajar on one side\". This is the most plausible defect among the options, even though it's subtle. <answer>C. The cap is slightly ajar on one side</answer>



Figure 13. A case study of the defect description task on the GoodsAD dataset.



**Question:**

There is a defect in the object. What is the potential effect of the defect?

A. Reduced performance  
 B. Improper insertion  
 C. Increased power consumption  
 D. Shorter lifespan

**Answer:**

The image shows an ultrasonic sensor module. A defect is visible: the header pins for the connector are bent or misaligned, particularly the middle pin. This physical defect can prevent the sensor from being properly inserted into a breadboard or PCB, leading to poor or no electrical connection. Let's analyze the options: A. Reduced performance: While possible, this is not the most direct effect of a bent pin. B. Improper insertion: This is a direct consequence of the bent pins. The pins cannot be inserted correctly into a socket or breadboard. C. Increased power consumption: Not directly related to the physical defect shown. D. Shorter lifespan: This is a potential long-term consequence, but not the immediate effect. The most immediate and direct effect of the bent pins is that the sensor cannot be properly inserted, which would prevent it from functioning correctly. <answer>B. Improper insertion</answer>



Figure 14. A case study of the defect analysis task on the Visa dataset.